# Condenser Microphone

A. Sheikh, J. Sakai, *Electrical and Computer Engineering, Carnegie Mellon*

***Abstract*—For the application of accurate voice reproduction, a simple condenser microphone design is considered. Analysis of theoretical characteristics is presented. Some insights regarding the design of the microphone are considered.**

***Keywords*—Capacitive, Condenser, Microphone.**

## I. Introduction

THE accurate transduction of sound into an electrical signal is naturally useful for conveying the human voice. People generally speak at 40 to 60 dB SPL and can hear sound from 20 Hz up to 20 kHz with especial sensitivity to the 1 to 4 kHz region.[1] For the application of accurate sound reproduction, the designer should strive for unity-gain response in these ranges, particularly in the 1 to 4 kHz range.

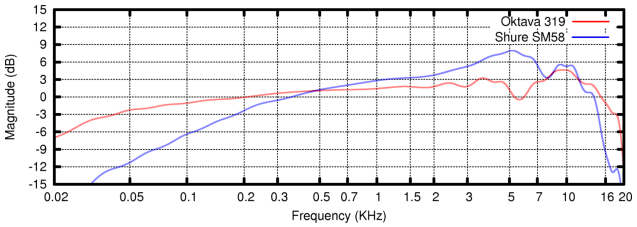


Fig. 1: *Oktava MK-319 condenser microphone*[2] *and Shure SM58 dynamic microphone*[3] *(20 Hz to 20 kHz)*

A variety of devices exist for transducing sound. Of commercially viable designs, condenser and dynamic microphones are the most common.[4] Fig. 1 plots the responses of a condenser microphone and a dynamic microphone. The condenser mic (in red) experiences less attenuation at the extremes and provides greater uniformity in between. It is not unusual for condenser mics to have an upper 20 kHz frequency limit compared to the typical 16 kHz limit experienced by dynamic mics.[5] Additionally, the condenser microphone has notably less gain in the 1 to 4 kHz region people are most sensitive to, providing a more balanced response. Generalizing these results, condenser microphones are preferable for applications desiring accurate reproduction.

## II. Sensor Structure and Measurement Principle

The diaphragm portion of the condenser microphone has a cylindrical form-factor. Its cross-section is depicted in Fig. 2. The diaphragm itself is a thin, tensioned membrane which is responsive to sound pressure in the target frequency range. The back-plate is a rigid structure with distributed perforations leading to an internal cavity. Between the membrane and the back-plate is the air-gap which forms the condenser dielectric. An acoustic resistance at the rear of the internal cavity serves as a normalizing vent, allowing the cavity to equalize to atmospheric pressure $P_0$.

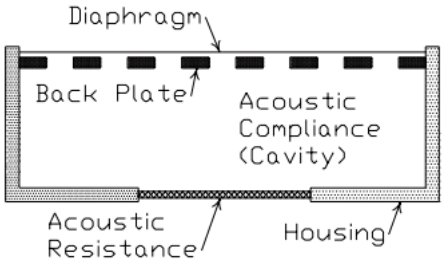


Fig. 2: *Diaphragm system cross-section*[6]

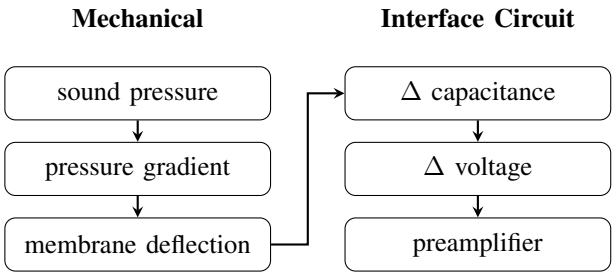


Fig. 3: *Transducer signal chain, first the mechanical process, then the interface circuit*

Condenser microphones convert sound pressure into a change in capacitance by the process shown in Fig. 3. Sound pressure gives rise to a pressure gradient which causes deflection across the condenser diaphragm. Membrane deflection in turn causes the capacitance of the condenser to vary.

| Symbol | Description |
|---|---|
| $r$ | radius in cylindrical coordinates |
| $R_M$ | membrane radius |
| $d_M$ | membrane thickness |
| $w$ | deflection along $z$-axis at a radius $r$ |
| $w_0$ | apex deflection, equal to $w(r=0)$ |
| $\Delta p_v$ | change in pressure caused by bias voltage |
| $E_M$ | Young's Modulus of elasticity (membrane) |
| $v_M$ | Poisson's ratio (membrane) |
| $h$ | dielectric air-gap |

Fig. 5: *Symbols used to model membrane deflection and calculate capacitance*

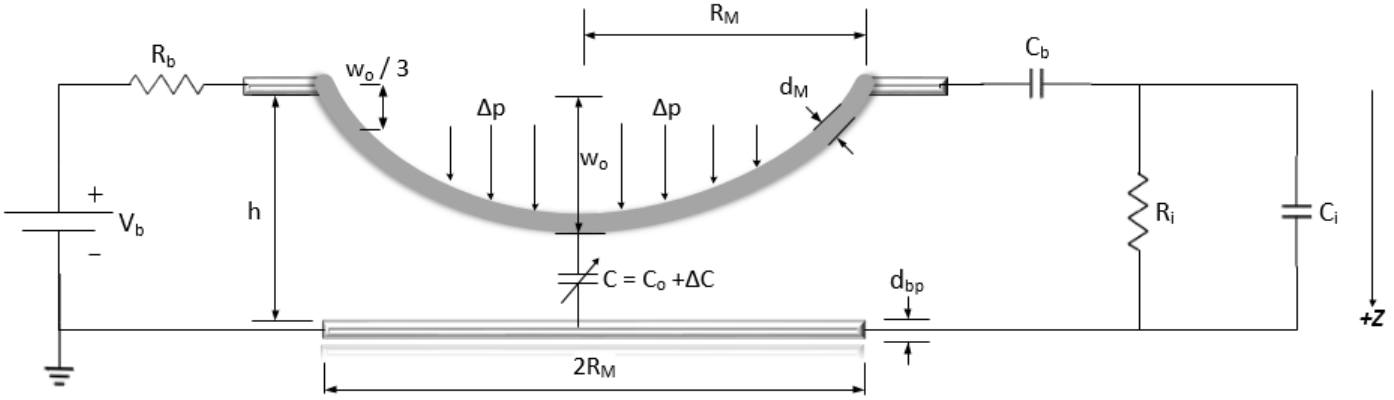


Fig. 4: *Mechanical diaphragm system undergoing deflection while coupled to first part of interface circuit*

### A. Membrane Deflection Due to Impinging Sound Pressure

Assuming that

1) membrane residual stress $\sigma_{M,0} = 0$
2) pressure $\Delta p$ is uniform across the membrane
3) the membrane's movement is purely along the $z$-axis

The apex deflection $w_0$ can be found using Eq. 2.[7]

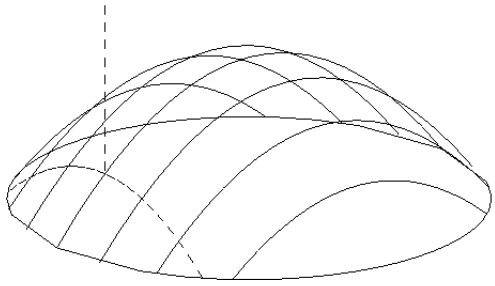

Fig. 6: *Membrane deflection modeled as a circular paraboloid*

$$w(r) = w_0 \left(1 - \frac{r^2}{R_M^2}\right) \tag{1}$$

$$\Delta p = \frac{4 w_0 d_m}{R_M^2} \frac{E_M}{1 - v_M^2} \left(\frac{4}{3}\frac{d_M^2}{R_M^2} + \sigma_0 + \frac{64}{105}\frac{w_0^2}{R_M^2}\right) \tag{2}$$

### B. Deflection Due to Bias Voltage

Keeping the membrane at $z = 0$, let the back-plate be held a distance $h$ away from the membrane at $z = h$ to create the dielectric air-gap. Applying a DC bias voltage $V_b$ between the membrane and back-plate causes opposing surface charges to form on the plates. By Coulomb's law, these surface charges attract and produce an electrostatic force $F_v$ on the membrane described by Eq. 3.[8] This force varies with the radius and is greater closer to the apex of deflection at $r = 0$. Simplifying the force to be uniform across the membrane allows it to be described in Eq. 4 as a uniform pressure $\Delta p_v$.[8]

$$F_v = \frac{1}{2} V^2 \frac{\epsilon_0 \pi R_M^2}{(h - w_v)^2} \tag{3}$$

$$\Delta p_v = \frac{1}{2}\epsilon_0 \left(\frac{V_b}{h}\right)^2 \tag{4}$$

### C. Capacitance

When only the bias voltage $V_b$ is applied, Eq. 5 relates how the pressure due to voltage $\Delta p_v$ produces an apex deflection $w_{v,0}$ towards the back-plate.[8] Letting $w_0 = w_{v,0}$ in Eq. 1 yields Eq. 6, an expression $w_v(r)$ for the deflection due to the bias voltage at any radius $r$.

$$w_{v,0} = \frac{\Delta p_v R_M^2}{4T} \tag{5}$$

$$w_v(r) = w_{v,0} \left(1 - \frac{r^2}{R_M^2}\right) \tag{6}$$

The modeled deflection $w_v(r)$ can be used to calculate the total condenser capacitance using the differential relationship shown in Eq. 7. The differential relationship models the condenser as a collection of parallel-plate capacitors having capacitance $dC$ and area $dA = r\, dr\, d\theta$. Integrating over the area of the membrane yields the expression for capacitance shown in Eq. 8. Using Eq. 9 to formulate a second-order ($n = 2$) series approximation for $\ln(x)$, the logarithm in Eq. 8 can be approximated to Eq. 10.[8] The value $C_0$ denotes the capacitance when there is no membrane deflection due to sound, $w_0 = 0$.

$$dC = \frac{\epsilon_0\, dA}{h - w_v} = \frac{\epsilon_0\, r\, dr\, d\theta}{h - w_{v,0}} \tag{7}$$

$$C = \frac{\epsilon_0 \pi R_M^2}{w_{v,0}} \ln\left|\frac{h}{h - w_{v,0}}\right| \tag{8}$$

$$\ln(x) = \sum_{n=1}^{\infty} \frac{(-1)^{n+1}}{n}(x-1)^n \tag{9}$$

$$C = \frac{\epsilon_0 \pi R_M^2}{h - w_v}\left(1 - \frac{1}{2}\frac{w_v}{h - w_v}\right) \tag{10}$$

## III. Interface Circuit

The interface circuit is the portion of the design responsible for converting variations in capacitance across the condenser into a low impedance voltage signal. It does so in two steps, as shown in Fig. 3. First the AC small-signal is extracted to obtain a high output impedance voltage signal using the coupling circuit in Fig. 4. This signal is then transformed into a low output impedance voltage signal using a preamplifier. The final signal can be sent much longer distances without noticeable degradation.[9]

Fig. 7 represents the small-signal equivalent model of Fig. 4. The interface circuit is inherently non-linear, so analyzing its small-signal equivalent model is an effective method of linearizing the relationship between capacitance and output voltage. In the small-signal equivalent model:

1) The DC-blocking coupling capacitor $C_b$ is shorted;
2) The polarizing DC-only voltage source $V_b$ is shorted;
3) The condenser's varying capacitance $\Delta C$ itself is modeled as a small-signal current source $i_c$.

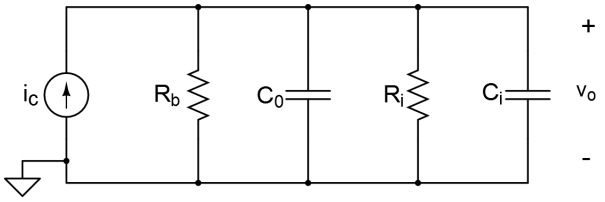


Fig. 7: *Small-signal equivalent model of interface circuit*

Note that when the polarizing voltage $V_b$ is shorted in the small-signal model, current-limiting resistor $R_b$ is now in parallel with the other devices in the interface circuit, particularly because coupling capacitor $C_B$ is modeled as a short in the small-signal model. Thus, since all elements are in parallel, no additional analysis (Miller approximations, for example) will be necessary. The result is a simplified Norton circuit with small-signal source seen in Eq. 11 and impedance seen in Eq. 12.

Leading to Eq. 13

By Ohm's Law and principles of source transformation, we derive the voltage output $v_o$, represented by Eq.15. The frequency-independent voltage at the output, then, is simply the magnitude of this.

$$i_c = (j\omega\Delta C)V_b \tag{11}$$

$$Z_{eq}(s) = Z_{R_{eq}} || Z_{C_{eq}} = \left(\frac{R_{eq}}{1 + sR_{eq}C_{eq}}\right) \tag{12}$$

$$R_{eq} = R_b || R_i \tag{13}$$

$$C_{eq} = C_0 + C_i \tag{14}$$

We must also consider the frequency response, as the most important bands of interest must be present at the output. In Eq. 17, we determine a low-frequency cutoff.

It's necessary to cascade this circuit into a pre-amplifier. Rather than for gain, this stage is primarily for impedance matching purposes. The following diagram exhibits a pre-amplifier that, for our purposes, is built from the MAX4466 operational amplifier.

Note that in this configuration, $R_i$ in our small-signal model is encapsulated by the $1M\Omega$ self-biasing resistors in parallel, since the DC-only power source is shorted in a small-signal analysis. These self-biasing resistors are large to match impedance with the very large input resistance at the op-amp pins. We also assume that $C_i = 0$. The current-limiting resistor $R_b$ is realized with the two $2k\Omega$ resistors and coupling capacitor $C_b$ is realized with the $0.01\mu F$ DC-blocking capacitor.

It's clear that the voltage at the inverting pin can be expressed as a division of admittances. Here we have a non-inverting operational amplifier configuration with a potential divider network between $Z_-$ and $Z_f$. The transfer in signal can be expressed with Eq. 21.

Thus, the low-frequency (DC) closed-loop gain $A_{CL}$ using $R_f = 100k\Omega$ and $R_- = 10k\Omega$ is simply 11 as demonstrated in Eq. 22.

It's commonly accepted to assume the output impedance of a non-inverting operational amplifier configuration is very low, and sometimes approximated as $0\Omega$. From a more analytical approach, we can derive an expression for the exact output impedance, as seen in Eq. 23. Note that, for the Max4465, the open-loop gain is typically $A_{VOL} = 95dB = 56,000V/V$.

$R_0$ is an internal resistance intrinsic to the amplifier, and note that $A_{VOL}$ greatly exceeds $A_{CL}$, yielding an output impedance that is low and can drive a range from $17\Omega$ to $300\Omega$ with acceptable power transfer.

## IV. Sensor Characteristics

Unless otherwise noted, the equations presented in the following section are derived using *AIP Handbook of Condenser Microphones*, see Ref. [8]. The electrical transfer function of the biased condenser when there is no deflection due to sound is given by Eq. 24.

### A. Sensitivity

The sensitivity of the microphone is given by Eq. 25 where $T$ represents the membrane tension. Based on Eq. 24 and

$$v_o(s) = i_c(Z_{eq}(s)) = \frac{\Delta C}{C_{eq}} V_b \frac{sR_{eq}C_{eq}}{1 + sR_{eq}C_{eq}} \tag{15}$$

$$v_O = \frac{\Delta C}{C_{eq}} V_b = \frac{\Delta C}{C_0} \left(1 + \frac{C_i}{C_0}\right) V_b \tag{16}$$

$$f_c = \frac{1}{2\pi R_{eq} C_{eq}} \tag{17}$$

Eq. 25, it is evident that the membrane radius can greatly affect the microphone sensitivity. This can be affirmed by the observation that larger diaphragm microphones have greater sensitivity than smaller ones. Intuitively, increasing membrane tension decreases the sensitivity of the sensor by limiting the movement of the membrane.

### B. Dynamic Range

The Maxim MAX4466 is the chosen amplifier for this design. Its datasheet indicates it has a 200 kHz operating bandwidth. In contrast, the condenser's operating bandwidth has an upper-limit around the vacuum resonant frequency of the membrane. This is given by Eq. 26 where $\sigma_M$ is the surface mass density of the diaphragm membrane.

It is clear from Eq. 26 that a larger bandwidth can be attained with higher tension, smaller membrane radius, and a thinner membrane with a lower surface mass density. Many condenser microphones, including the Oktava MK-319 in Fig. 1 have a mechanical resonant peak around 10 kHz.

### C. Sensitivity to Temperature

Within the diaphragm system, thermal expansion of the diaphragm membrane due to an increase in temperature causes a reduction in membrane tension $T$. By Eq. 25, this behavior increases the sensitivity but decreases the bandwidth. An increase in temperature additionally produces a corresponding increase in air viscosity. This physical feature of air is important primarily around the mechanical resonant frequency as it causes higher damping which in turn results in a lower and broader resonant peak.

Temperature increases also affect air density and subsequently the mechanical-acoustic properties of the diaphragm system, namely the acoustic compliances.

The composite result of the above temperature effects is a low sensitivity to temperature, typically on the order of $-0.005$ dB/K.

The amplifier datasheet shows the op-amp performance across a range of temperatures. As the implicit use for the microphone presented in this article is around room temperature, focus is given to the temperature range of 293K to 300K. Within this region, the op-amp's temperature dependency is quite linear. The most notable impact of temperature is its effect on large-signal gain which decreases by approximately $-0.35$ dB/K in this region.

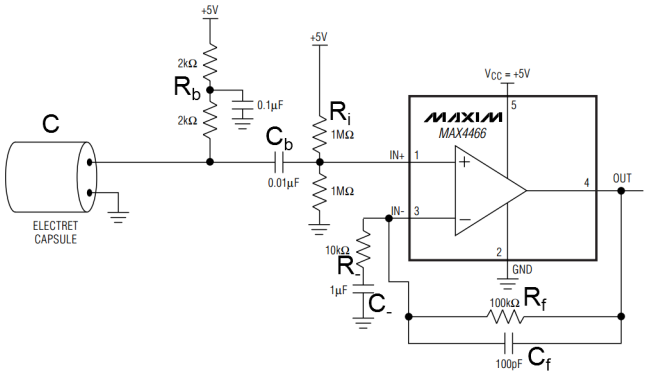


Fig. 8: *Amplifier stage (seen on the right)*

$$V_- = V_{out} \frac{G_f}{G_- + G_f} \tag{18}$$

$$G_- = (Z_-)^{-1} = \frac{sC_-}{1 + sR_-C_-} \tag{19}$$

$$G_f = (Z_f)^{-1} = sC_f + \frac{1}{R_f} \tag{20}$$

$$A_v = 1 + \frac{Z_f}{Z_-} \tag{21}$$

### D. Noise Analysis

Johnson noise has a power spectral density (PSD) according to the Nyquist formula shown in Eq. 27 where $T$ is the temperature in degrees Kelvin. The pressure spectral density (pSD) is simply the square-root of the PSD. Results from Eq. 27 can be used to calculate the RMS noise pressure experienced by the microphone. Calculations are given with $\Delta f = 10$ kHz. Preamplifier noise is taken directly from the preamplifier datasheet and displayed in Fig. 10.

## V. Conclusion

The condenser microphone's theoretical analysis yields expressions for the system capacitance, voltage output and sensitivity based on geometries. These equations can be used to gain insight about how to improve the operation of the microphone, e.g. increased the membrane radius to increase sensitivity.

$$A_{CL} = 1 + \frac{R_f}{R_-} = 11 \tag{22}$$

$$R_{out} = R_0 \frac{A_{CL}}{A_{VOL}} \tag{23}$$

| Symbol | Description | Typ. Value |
|---|---|---|
| $\sigma_M$ | surface mass density | $4.45 \times 10^{-2}$ kg/m$^2$ |
| $T$ | room temperature | 300 K |
| $k_B$ | Boltzmann constant | $1.38 \times 10^{-23}$ J/K |
| $R_A$ | damping resistance | $2 \times 10^7$ N$\cdot$s/m$^5$ |

Fig. 9: *Symbols used in analyzing sensor characteristics*

$$M_e = \frac{1}{2}\frac{V_b}{h - w_0} \cdot \left[1 + \frac{C_i}{C_0}\right]^{-1} \tag{24}$$

$$M_p = M_e \cdot \frac{R_M^2}{8T} \tag{25}$$

$$f_H = \frac{2.4048}{2\pi R_M}\left(\frac{T}{\sigma_M}\right)^{1/2} \tag{26}$$

$$PSD = (pSD)^2 = \frac{p_{rms}^2}{\Delta f} = 4k_B T R_A \ [\text{Pa}^2/\text{Hz}] \tag{27}$$

$$\begin{aligned} PSD &= 4 \times 1.38 \times 10^{-23} \times 300 \times 2 \times 10^7 \\ &= 3.3 \times 10^{-13} \text{ Pa}^2 \text{ Hz} \\ pSD &= \sqrt{3.3 \times 10^{-13}} = 5.75 \times 10^{-7} \text{ Pa Hz}^{1/2} \\ p_{rms} &= 5.75 \times 10^{-7} \times \sqrt{10^4} = 5.75 \times 10^{-5} \text{ Pa} \end{aligned}$$

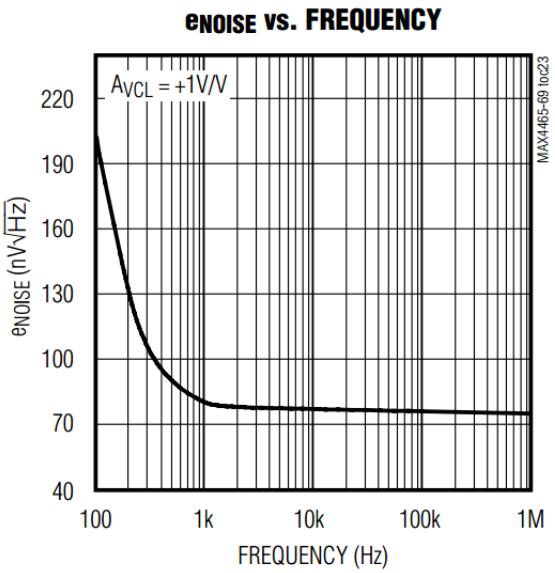


Fig. 10: *Noise vs. frequency for Maxim MAX4466 preamplifier, taken directly from datasheet*[10]

## REFERENCES


[1] S. W. Smith, *The Scientist and Engineer's Guide to Digital Signal Processing*, First. San Diego, CA 92150-2407, USA: California Technical Publishing, 1997, ISBN: 0-9660176-3-3.

[2] Oktava GmbH. (2014). Oktava mk-319 condenser microphone, [Online]. Available: http://www.oktava-online.com/mk319.htm (visited on 04/20/2014).

[3] Shure Inc. (2014). SM58 Vocal Microphone, [Online]. Available: http://www.shure.com/americas/products/microphones/sm/sm58-vocal-microphone (visited on 04/20/2014).

[4] J. Shambro. (2014). Condenser vs. dynamic microphones, [Online]. Available: http://homerecording.about.com/od/microphones101/a/mic_types.htm (visited on 02/24/2014).

[5] P. White. (Apr. 1998). Mic types & characteristics, [Online]. Available: http://www.soundonsound.com/sos/apr98/articles/mic_types.html (visited on 02/24/2014).

[6] G. Torio and J. Segota, "Unique directional properties of dual-diaphragm microphones," 5179, Audio Engineering Society, Evanston, Illinois 60202, USA, Sep. 2000. [Online]. Available: http://www.aes.org/sections/chicago/AES_LA_6_21_00.PDF.

[7] W. K. Schomburg, "Membranes," in *Introduction to Microsystem Design*, Berlin: Springer-Verlag, 2011, pp. 29–50.

[8] T. F. Wong George S.K.; Embleton, *AIP Handbook of Condenser Microphones: Theory, Calibration and Measurements*. 500 Sunnyside Boulevard, Woodbury, NY 11797-2999: American Institute of Physics, 1997, ISBN: 1563962845.

[9] Brel & Kjr, *Microphone handbook, vol. 1: theory*, BE 144711, Nrum, Denmark: Brel & Kjr, 1996. [Online]. Available: http://www.bksv.com/doc/be1447.pdf (visited on 04/29/2014).

[10] Maxim Integrated Products, *MAX4465-MAX4469*, Apr. 2001. [Online]. Available: http://www.adafruit.com/datasheets/MAX4465-MAX4469.pdf.